Numerical prediction of size, mass, temperature and trajectory of cylindrical wind-driven firebrands

Article *in* International Journal of Wildland Fire · January 2014

DOI: 10.1071/WF13080

5 authors, including:

L. A. Oliveira
University of Coimbra
30 PUBLICATIONS **540** CITATIONS
SEE PROFILE

Antonio Gameiro Lopes
University of Coimbra
121 PUBLICATIONS **1,322** CITATIONS
SEE PROFILE

Miguel Almeida
University of Coimbra
78 PUBLICATIONS **376** CITATIONS
SEE PROFILE

Domingos X. Viegas
University of Coimbra
357 PUBLICATIONS **5,830** CITATIONS
SEE PROFILE

CSIRO PUBLISHING

International Journal of Wildland Fire **2014**, *23*, 698–708
http://dx.doi.org/10.1071/WF13080

Numerical prediction of size, mass, temperature and trajectory of cylindrical wind-driven firebrands

Luis A. Oliveira[A,C], *António G. Lopes*[A], *Bantwal R. Baliga*[B], *Miguel Almeida*[A] *and Domingos X. Viegas*[A]

[A]ADAI/LAETA, Department of Mechanical Engineering (FCTUC – Polo II), University of Coimbra, PT-3030-201 Coimbra, Portugal.
[B]Department of Mechanical Engineering, McGill University, 817 Sherbrooke Street, West Montreal, QC, H3A 0C3, Canada.
[C]Corresponding author. Email: luis.adriano@dem.uc.pt

Abstract. Mathematical models and numerical solution procedures for predicting the trajectory, oscillation, possible rotation, and mass and size time-evolution of cylindrical wind-driven firebrands are described and discussed. Two test problems and the results, used for validating the mathematical models, are presented. In one, experimental measurements of non-burning cylindrical particles falling in still air are compared to numerical predictions and in the other, predictions of time-evolution of mass and size of stationary burning particles in air flows are compared with experimental results reported in the literature. Results yielded by the proposed models for a demonstration problem involving cylindrical wind-driven firebrands, with the same initial volume, mass and position, but different initial aspect ratios and distinct initial orientations relative to the wind velocity, are then presented. These results show the following: the horizontal distance travelled by the firebrand from release to landing locations is an increasing function of its initial aspect ratio; and the initial orientation of the firebrand, and its subsequent oscillations including possible rotation, have a significant influence on its trajectory, thus it is important to account for them in mathematical models formulated for predicting the spread of fires by spotting.

Additional keywords: horizontal distance travelled, mathematical models, oscillations, rotations, spot fires, total falling time, trajectories.

Received 21 March 2012, accepted 20 March 2014, published online 27 June 2014

Introduction

Wildland crown and surface fires are often spread by spotting: burning pieces of forest vegetation (firebrands) are lofted by a fire plume and transported by the prevailing wind, as shown schematically in Fig. 1 (adapted from Sardoy *et al.* 2006). When these firebrands land, they may ignite new fires at locations that can be up to a few kilometres from the main fire. Understanding this fire propagation process is particularly important for the planning of wildland fire suppression as well as for prescribed burning operations.

The desire and need to understand and control the spread of fires caused by spotting has motivated a large number of related research works. These include experimental and field studies (McArthur 1967; Ellis 2000; Ohmiya and Iwami 2000; Knight 2001; Manzello *et al.* 2007, 2008, 2010, 2011, 2012*a*, 2012*b*; Suzuki *et al.* 2012; Sullivan *et al.* 2013), and also the development and use of mathematical models for predicting the spread of fires by spotting (Viegas 2002, 2004, 2006; Mell *et al.* 2009; Sullivan 2009*a*, 2009*b*, 2009*c*; Koo *et al.* 2010).

In many of the available models for predicting fire spread by spotting, the firebrands are often approximated as burning cylinders or disks (Tarifa *et al.* 1965; Tse and Fernandez-Pello 1998; Anthenien *et al.* 2006; Sardoy *et al.* 2006, 2007, 2008; Kortas *et al.* 2009; Albini *et al.* 2012; Koo *et al.* 2012). Some of these works, for example, Sardoy *et al.* (2006, 2007, 2008), present detailed mathematical models and numerical predictions of the fire plume, the wind-flow field and the motion and burning of the firebrands. In contrast, in Tarifa *et al.* (1965), Tse and Fernandez-Pello (1998), Anthenien *et al.* (2006), Almeida *et al.* (2009) and Kortas *et al.* (2009), comparatively simpler but more practical models, which invoke semi-empirical correlations based on experimental data, are used for numerical predictions of firebrand trajectories and of the rates of mass and volume reduction due to the combustion. In such models, including the recent works of Albini *et al.* (2012) and Koo *et al.* (2012), it is usually assumed that the firebrands align themselves and remain in an orientation of maximum drag. For a cylindrical firebrand, this assumption means that the major axis of the cylinder always remains perpendicular to the relative velocity vector, and the influence of particle oscillations (and possible rotation) on its trajectory and burning rate are considered to be negligibly small. This assumption considerably

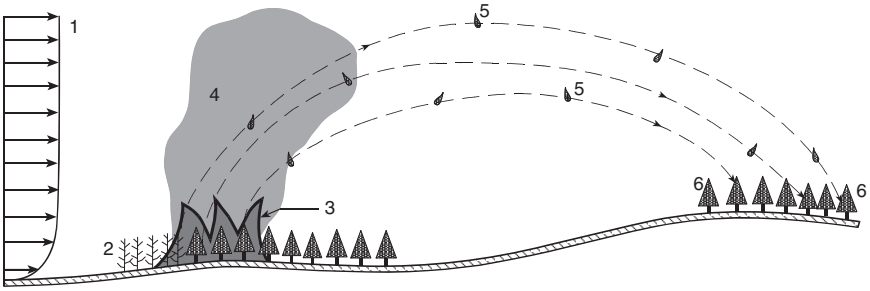

Fig. 1. Schematic illustration of the spotting process: 1, wind profile; 2, burned vegetation; 3, main fire; 4, plume; 5, firebrands; and 6, receptive fuel bed.

simplifies the overall particle-tracking procedure, but it may not be justifiable under certain circumstances.

Woycheese and Pagni (1999) reviewed eight different burning models for disk-shaped wood firebrands lofted in a fire plume and propagated downwind. They demonstrated the importance of including both lift and drag, but their simulations were done for several different fixed angles of attack (in the range 35–90°) in relation to the relative velocity vector (but did not model firebrand oscillations). Himoto and Tanaka (2005) proposed a model for disk-shaped wind-driven firebrands, in which three-dimensional unsteady equations of linear and angular momentum are solved simultaneously (accounting for drag, lift and gravitational forces, and also firebrand orientation and oscillations). However, they prescribed the drag, lift and moment coefficients as functions of the angle of attack with respect to the relative velocity vector, using curve fits to the experimental data of Tachikawa and Fukuyama (1981) at a fixed Reynolds number of 40 000, and did not consider combustion of the firebrand.

The present work is concerned with predictions of the trajectories of wind-driven burning cylindrical firebrands, after they are released from the fire plume, using relatively simple and practical mathematical models. In particular, the focus is on evaluating the possible influence of the initial orientation and the subsequent oscillations (and possible rotation) of the burning cylindrical firebrand on its trajectory. The drag, lift and gravitational forces are taken into account in the linear momentum equation of the firebrand, borrowing and extending ideas from the works of Hoerner (1965), Yin *et al.* (2003, 2004), Oliveira *et al.* (2008), Kortas *et al.* (2009), Kelbaliyev (2011) and Ren *et al.* (2011). In the angular momentum equation, the effects of pitching moment (caused by non-coincidence of the centre of mass and centre of pressure) and aerodynamic resistance to the oscillation (and rotation) of the firebrand are taken into account, using ideas put forward by Yin *et al.* (2003, 2004), Hölzer and Sommerfeld (2008), and Mandø and Rosendhal (2010). The combustion model used in this work is akin to that proposed by Anthenien *et al.* (2006).

Validations of the proposed mathematical models are done using two test problems: in one, numerical predictions of falling non-burning cylindrical particles in still air are compared with measurements from an indoor experimental investigation that was undertaken as a part of this work; and in the other, numerical predictions of the mass and size of stationary burning particles in an air tunnel are compared with the corresponding experimental results reported in Tarifa *et al.* (1965, 1967) and Anthenien *et al.* (2006). Following these validation tests, the results yielded by the proposed models for a demonstration problem involving wind-driven, cylindrical, burning firebrands are used to assess the importance of including the effects of initial particle orientation, oscillations and rotation in predictions of fire spread by the spotting process.

Methodology

Mathematical models for wind velocity distribution, motion of the cylindrical firebrands and burning of these firebrands are described in this section. A note on the numerical solution of these models is also included at the end of this section.

Wind velocity distribution

Winds prevailing over a forest fire, and the buoyant plume above the fire, are influenced by weather, surface topography and types of fuel (trees and other vegetation), and also by the size, shape and power of the fire (Lopes *et al.* 1995; Porterie *et al.* 2005; Viegas 2004, 2006; Sardoy *et al.* 2007; Zhou *et al.* 2007; Mell *et al.* 2009). However, the main aims of this work (stated in the previous section) could be achieved by limiting attention to winds over a flat terrain and assuming that the effects of temperature stratification are negligible. In this context, the time-mean wind velocity vector is in the horizontal plane. With respect to the Cartesian coordinate system shown in Fig. 2*a*, this wind velocity vector is aligned with the positive x-direction and expressed as follows (Tse and Fernandez-Pello 1998; Ahrens 2009):

$$\vec{V}_W = V_{W,x}\vec{i} + V_{W,y}\vec{j} + V_{W,z}\vec{k};\ \text{with}\ V_{W,y} = V_{W,z} = 0,\ \text{and}$$
$$V_{W,x} = \begin{cases} \dfrac{V_{ref}}{\kappa}\ln\left(\dfrac{z}{z_o}\right) & \text{for } z \geq z_o \\ 0 \text{ for } z < z_o \end{cases} \quad (1)$$

In Eqn 1, z is the vertical distance from the ground; z_o is a roughness height; $\kappa = 0.40$ is the von Karman constant; and V_{ref} is a reference value that is used to prescribe the wind speed ($|\bar{V}_W|$) at some reference height, for example, 10 m above the ground (Tse and Fernandez-Pello 1998; Anthenien *et al.* 2006). McRae *et al.* (1982) give the following values of roughness height: $z_o = 0.05$ m for uncut grass; $z_o = 0.1$ m for fully grown root crops and $z_o = 1.0$ m for tree-covered terrain.

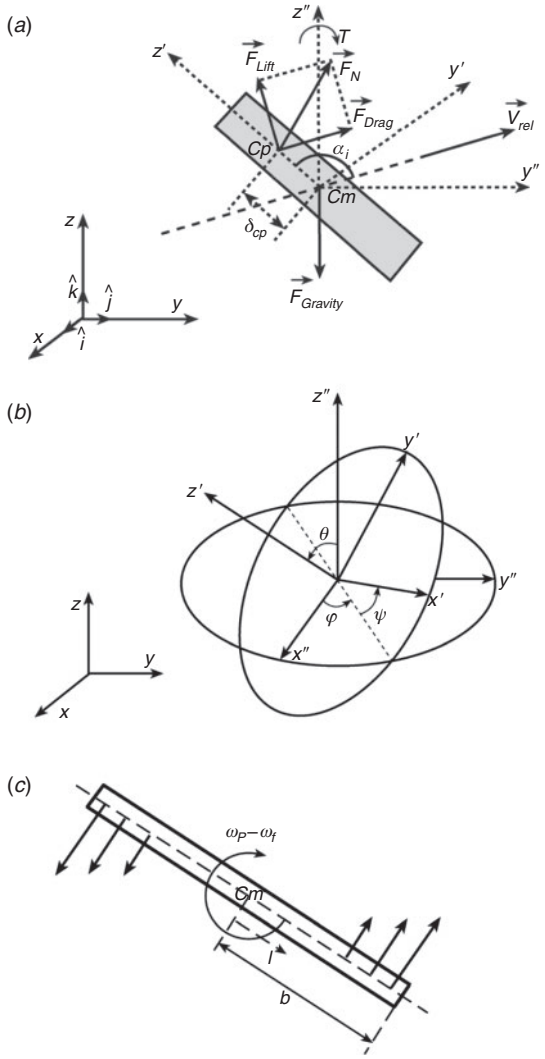

Fig. 2. Schematic illustrations of (*a*) Cartesian coordinate systems, normal force, drag force, lift force and related notation; (*b*) Euler angles and (*c*) notation and velocities in the model for the aerodynamic resistance torque opposing the rotation of the particle.

Motion of cylindrical firebrands

The firebrands considered in the present work are solid cylinders with radius '*a*' and half-length '*b*' (aspect ratio $\beta = b \div a$). The coordinate systems and notations that are used to describe their translational and rotational motions are schematically illustrated in Fig. 2*a*. In this figure, $\vec{x} = [x, y, z]$ denotes a position vector in an inertial Cartesian coordinate system with its origin anchored on the ground directly beneath the initial position of the firebrand, the positive *x*-direction aligned with the main wind direction and the positive *z*-direction pointing vertically upwards (the gravitational force on the firebrand, $\vec{F}_{Gravity}$, points in the negative *z*-direction); $\vec{x}' = [x', y', z']$ is the position vector in a Cartesian coordinate system that has its origin fixed to the firebrand centre of mass (*Cm*) and its axes aligned with the principal axes of the particle and co-rotating with it (referred to as the particle frame); and $\vec{x}'' = [x'', y'', z'']$ is a position vector associated with a Cartesian coordinate system with its origin fixed to *Cm* and axes parallel to those of the aforementioned inertial frame. The relative velocity vector is $\vec{V}_{rel} = \vec{V}_W - \vec{V}_P$, where $\vec{V}_W$ and $\vec{V}_P$ are the velocities of the wind and particle centre of mass.

The translational and rotational motions of the firebrand are respectively modelled using Eqns 2 and 3–5 (Yin *et al.* 2003, Mandø and Rosendhal 2010):

$$m_P \frac{d\vec{V}_P}{dt} = \vec{F}_{Drag} + \vec{F}_{Gravity} + \vec{F}_{Pressure\ Gradient} + \vec{F}_{Virtual\ Mass} + \vec{F}_{Lift} + \vec{F}_{Basset\ history} \quad (2)$$

$$I_{x'} \frac{d\omega_{x'}}{dt} - \omega_{y'}\omega_{z'}(I_{y'} - I_{z'}) = T'_{x'} \quad (3)$$

$$I_{y'} \frac{d\omega_{y'}}{dt} - \omega_{z'}\omega_{x'}(I_{z'} - I_{x'}) = T'_{y'} \quad (4)$$

$$I_{z'} \frac{d\omega_{z'}}{dt} - \omega_{x'}\omega_{y'}(I_{x'} - I_{y'}) = T'_{z'} \quad (5)$$

In Eqn 2, m_P, $\vec{V}_P\vec{F}$ and t are the instantaneous mass of the particle, the velocity vector of its centre of mass in the inertial frame, the forces acting on it and time. In Eqns 3–5, $[I_{x'}, I_{y'}, I_{z'}]$ are the moments of inertia with respect to the particle principal axes, with $I_{x'} = I_{y'} = m_P\, a^2 \div 4 + m_P\, b^2 \div 3$ and $I_{z'} = m_P\, a^2 \div 2$; $[\omega_{x'}, \omega_{y'}, \omega_{z'}]$ and $[T'_x, T'_y, T'_z]$ are the angular velocity components and the components of the torque acting on the particle, all written in the particle frame. In summary, particle translation is expressed in the inertial frame, whereas its rotation is referred to the particle frame.

After the firebrands are ejected from their parent tree, they are lofted by the buoyant plume over the main fire, which aligns with the main crosswind. In this work, attention is focussed only on firebrands that have been carried by the plume to their maximum height. Subsequent trajectories of such firebrands are determined by the prevailing wind and not by the plume. Thus, in the proposed model, at the starting position, each firebrand is injected into the wind with height and initial velocity in suitably chosen ranges. Furthermore, the air–solid density ratio is very low, so the pressure gradient, virtual mass and Basset history forces in Eqn 2 are negligible compared to drag, gravity and lift forces. Moreover, the particle motion is assumed to have negligible influence on the wind velocity distribution. This assumption is acceptable as a consequence of the very low particle concentration in the problems of interest. It is also assumed that the rate of mass loss from the surface of the firebrands is essentially uniform: thus, the net force associated with this rate of mass loss (or ejection) from each firebrand is negligible.

Using the 'cross-flow principle' of Hoerner (1965), and the notation in Fig. 2*a*, for a very long cylinder (aspect ratio, β, approaching infinity), the magnitude of the force normal to the major axis (z') of the cylinder ($|\vec{F}_N|$) primarily depends only on the magnitude of the relative velocity in this direction ($|\vec{V}_{rel}|\sin\alpha_i$) and the corresponding dynamic pressure ($0.5\,\rho_{air,film}(|V_{rel}|\sin\alpha_i)^2$). The subscript 'film' associated with the properties of air (here and elsewhere in the

paper) is used to indicate that their values are evaluated at the prevailing atmospheric pressure and the film temperature, $T_{film} = (T_P + T_{air,\infty}) \div 2$. In this work, all of the required properties of air were calculated using correlations obtained by curve-fitting data given in Incropera and DeWitt (1996). Thus, introducing a drag coefficient, C_D (elaborated later in this section), $|\vec{F}_N| = C_D[D_P(2b)]\,[0.5\,\rho_{air,film}(|\vec{V}_{rel}|\sin\alpha_i)^2]$. Furthermore, the magnitudes of the viscous and pressure forces in the direction of the major axis of the cylinder are assumed to be negligible, compared to $|\vec{F}_N|$. Thus, $\vec{F}_N = \vec{F}_{Drag} + \vec{F}_{Lift}$; $|\vec{F}_{Drag}| = |\vec{F}_N||\sin\alpha_i|$ and $|\vec{F}_{Lift}| = |\vec{F}_N||\cos\alpha_i|$; and the following equations apply:

$$\vec{F}_{Drag} = |\vec{F}_{Drag}|\frac{\vec{V}_{rel}}{|\vec{V}_{rel}|} = \rho_{air,film}\,C_D\,D_P\,b\,|\vec{V}_{rel}||\sin\alpha_i|^3\,\vec{V}_{rel} \quad (6)$$

$$\begin{aligned}\vec{F}_{Lift} &= |\vec{F}_{Lift}|\,\frac{\cos\alpha_i}{|\cos\alpha_i|}\,\frac{[\hat{z}'\times\vec{V}_{rel}]\times\vec{V}_{rel}}{|[\hat{z}'\times\vec{V}_{rel}]\times\vec{V}_{rel}|}\\ &= \rho_{air,film}\,C_D\,D_P\,b\,[|\vec{V}_{rel}|\sin(\alpha_i)]^2\cos\alpha_i\,\frac{[\hat{z}'\times\vec{V}_{rel}]\times\vec{V}_{rel}}{|[\hat{z}'\times\vec{V}_{rel}]\times\vec{V}_{rel}|}\end{aligned} \quad (7)$$

In Eqn 7, $\hat{z}'$ is the unit vector in the positive z' direction. The force due to gravity is $\vec{F}_{Grav} = Vol_P\,(\rho_P - \rho_{air,film})\vec{g}$, where $\vec{g}$ is the gravitational acceleration, ρ_P is the particle density and Vol_P is the instantaneous volume of the firebrand.

Expressions for the drag and lift coefficients, C_D and C_L, have been proposed in the literature by many authors, including Hoerner (1965), Ganser (1993), Yin *et al.* (2003), Hölzer and Sommerfeld (2008), Kelbaliyev (2011) and Ren *et al.* (2011). Equations adapted from these references were implemented and tested in the present work, and they yielded significantly different numerical results. Similar findings have been reported in the critical review of Mandø and Rosendhal (2010). Finally, after numerous tests and checks (particularly, with regard to reliable generation of firebrand oscillations and rotation) an adaptation of the drag coefficient proposed by Kelbaliyev (2011) for cylinders in cross-flow, together with the aforementioned cross-flow principle of Hoerner (1965), was adopted for calculations of the drag and lift forces. Based on the work of Kelbaliyev (2011), the following equation is proposed for calculating the drag coefficient:

$$C_D = \begin{cases} \dfrac{10}{(\mathrm{Re}_{\alpha_i})^{0.778}} \text{ for } \mathrm{Re}_{\alpha_i} < 0.1 \\ \dfrac{10}{(\mathrm{Re}_{\alpha_i})^{0.778}}\left(1 + 0.1076(\mathrm{Re}_{\alpha_i})^{0.778}\right) \\ \quad \text{for } 0.1 \le \mathrm{Re}_{\alpha_i} \le 6\times10^3 \\ 1.1 \text{ for } 6\times10^3 < \mathrm{Re}_{\alpha_i} \le 2\times10^5 \end{cases} \quad (8)$$

In Eqn 8, $\mathrm{Re}_{\alpha_i} = \rho_{air,film}\,D_P\,|\vec{V}_{rel}||\sin(\alpha_i)| \div \mu_{air,film}$.

The torque vector ($\vec{T}' = [\vec{T}'_{x'}, \vec{T}'_{y'}, \vec{T}'_{z'}]$) used in Eqns 3–5 includes two distinct effects: the pitching moment ($\vec{T}'_1$) and the rotational torque ($\vec{T}'_2$) caused by the influence of the corresponding aerodynamic resistance that is exerted on the cylindrical particle. The full resulting torque is thus given by $\vec{T}' = \vec{T}'_1 + \vec{T}'_2$.

As shown in Fig. 2*a*, δ_{Cp} denotes the distance between the centre of mass and the centre of pressure, measured along the particle principal axis (z'). This distance and the pitching moment, $\vec{T}_1$, in the inertial frame of reference, $\vec{x} = [x, y, z]$, are calculated using the following equations (Marchildon *et al.* 1964; Mandø and Rosendhal 2010):

$$\begin{aligned}\delta_{Cp} &= 2b[90 - \alpha_i]/(480)\\ \vec{T}_1 &= (\delta_{Cp}\,\hat{z}')\times(\vec{F}_{Drag} + \vec{F}_{Lift})\end{aligned} \quad (9)$$

The sign of δ_{Cp} (and thus the sign of $\vec{T}_1$) depends of the sign of $\cos\alpha_i$ (where α_i is measured in degrees), as the centre of pressure is always located on the leading-edge side of the cylindrical particle. For use in Eqns 3–5, the pitching moment ($\vec{T}_1$) in the inertial frame is transformed to $\vec{T}'_1$ in the particle frame as follows:

$$\vec{T}'_1 = A\,\vec{T}_1 = A\,(\delta_{Cp}\,\hat{z}')\times(\vec{F}_{Drag} + \vec{F}_{Lift}) \quad (10)$$

In this expression, A stands for the transformation matrix between the reference frames $\vec{x}'$ and $\vec{x}''$, illustrated in Fig. 2*a*: $\vec{x}' = A\,\vec{x}''$. The elements of this matrix are based on the Euler angles (θ, φ, ψ) illustrated in Fig. 2*b* and given by the following equation (Goldstein *et al.* 2002; Yin *et al.* 2003, 2004):

$$A = \begin{bmatrix} \cos\psi\cos\varphi - \cos\theta\sin\varphi\sin\psi & \cos\psi\sin\varphi + \cos\theta\cos\varphi\sin\psi & \sin\psi\sin\theta \\ -\sin\psi\cos\varphi - \cos\theta\sin\varphi\cos\psi & -\sin\psi\sin\varphi + \cos\theta\cos\varphi\cos\psi & \cos\psi\sin\theta \\ \sin\theta\sin\varphi & -\sin\theta\cos\varphi & \cos\theta \end{bmatrix} \quad (11)$$

The component $T'_{2,z'}$ of the rotational torque along the major axis, z', of the cylindrical particle is assumed to be negligibly small; and it also does not influence the particle oscillations or rotations that are of significance in this study. Furthermore, $I_{x'} = I_{y'}$; thus, using Eqn 5, it can be concluded that $\omega_{z'}$ would be negligible (so it is not calculated in this analysis). The components $T'_{2,x'}$ and $T'_{2,y'}$ are influenced by the relative rotation vector $\vec{\Omega} = \{0.5(\vec{\nabla}\times\vec{V}_{rel}) - \vec{\omega}_P\}\}$ (Zastawny *et al.* 2012). Here, $0.5(\vec{\nabla}\times\vec{V}_{rel})$ is an estimation of the local angular velocity of the relative velocity field ($\vec{\omega}_f$) and $\vec{\omega}_P$ is the angular velocity of the particle. In this work, $0.5(\vec{\nabla}\times\vec{V}_{rel})$ is assumed to be negligibly small. Noting that $T'_{2,x'}$ and $T'_{2,y'}$ *oppose* the rotation of the particle (as they are components of the aerodynamic resistance torque) and using the notation in Fig. 2*c*, the following expressions can be derived:

$$\begin{aligned}T'_{2,x'} &= -\rho_{air,film}|\omega_{x'}|\omega_{x'}D_P\left\{\int_0^b C_{D,y'}\,l^3\,dl\right\}\\ T'_{2,y'} &= -\rho_{air,film}|\omega_{y'}|\omega_{y'}D_P\left\{\int_0^b C_{D,x'}\,l^3\,dl\right\}\end{aligned} \quad (12)$$

A simplified version of the Kelbaliyev (2011) model, as expressed in Eqn 8, is used for the *local* rotational drag coefficients, $C_{D,x'}$ and $C_{D,y'}$ and, at the location, l, with respect to the particle centre of mass, as shown in Fig. 2*c*:

$$C_{D,x'} = 1.076 + 10/\{\rho_{air,film} D_P |\omega_{y'}| l/\mu_{air,film}\}^{0.778}$$
$$C_{D,y'} = 1.076 + 10/\{\rho_{air,film} D_P |\omega_{x'}| l/\mu_{air,film}\}^{0.778} \quad (13)$$

where $\rho_{air,film} D_P |\omega_{y'}| l/\mu_{air,film}$ is the Reynolds number based on the *local* velocity $|\omega_{y'}| l$ and $\rho_{air,film} D_P |\omega_{x'}| l/\mu_{air,film}$ is the is the Reynolds number based on the *local* velocity $|\omega_{x'}| l$.

Using these equations for $C_{D,x'}$ and $C_{D,y'}$, the integrals in the expressions for $T'_{2,x'}$ and $T'_{2,y'}$ are evaluated and the following equations are obtained:

$$T'_{2,x'} = -\rho_{film} |\omega_{x'}| \omega_{x'} ab^4 \left\{ 0.538 + 3.62 \left(\frac{\rho_{film} a |\omega_{x'}| b}{\mu_{film}} \right)^{-0.778} \right\}$$
$$T'_{2,y'} = -\rho_{film} |\omega_{y'}| \omega_{y'} ab^4 \left\{ 0.538 + 3.62 \left(\frac{\rho_{film} a |\omega_{y'}| b}{\mu_{film}} \right)^{-0.778} \right\} \quad (14)$$

With respect to the notation given in Fig. 2, the position of the centre of mass ($\vec{x}_P$) and the Euler angles (θ, φ, ψ) of the firebrand are obtained by integrating the following equations:

$$\frac{d\vec{x}_P}{dt} = \vec{V}_P; \quad \frac{d\theta}{dt} = \omega_{x'} \cos\psi - \omega_{y'} \sin\psi$$
$$\frac{d\varphi}{dt} = (\omega_{x'} \sin\psi + \omega_{y'} \cos\psi)/\sin\theta; \quad \frac{d\psi}{dt} = \omega_{z'} - \left(\frac{d\varphi}{dt}\right) \cos\theta \quad (15)$$

In practice, Euler parameters are used instead of Euler angles to avoid singularities in determining $d\varphi/dt$ (Goldstein *et al.* 2002; Yin *et al.* 2003).

When the firebrand is burning, its instantaneous diameter and mass reduce with time: semi-empirical models for these processes are discussed in the next subsection.

Burning of cylindrical firebrands

Models of various degrees of detail for the burning of woody (biomass) materials are available in the literature, for example, in the works of Roberts (1970), Muraszew and Fedele (1977), Woycheese and Pagni (1999), Yin *et al.* (2004), Porteiro *et al.* (2006) and Sardoy *et al.* (2006, 2007, 2008). However, Tse and Fernandez-Pello (1998) and Anthenien *et al.* (2006) have shown that relatively simple, but adequate (from a practical point of view), models of the rates of mass loss and size regression of firebrands can be obtained using curve fits to the experimental data of Tarifa *et al.* (1965, 1967) on the burning of stationary wood particles in an air tunnel. Their models were adapted for the numerical predictions undertaken in this work.

Following the particle-burning models of Tse and Fernandez-Pello (1998) and Anthenien *et al.* (2006), the outer surface of the firebrand is held at a fixed (constant) temperature as the pyrolysis front propagates radially inwards. Firebrand surface temperatures of 853 and 993 K are recommended in the works of Muraszew and Fedele (1977), Tse and Fernandez-Pello (1998) and Anthenien *et al.* (2006). In this work, however, for comparing predictions yielded by the proposed model with the experimental data of Tarifa *et al.* (1967) for stationary, burning, cylindrical particles of oak in a wind tunnel, the particle surface temperature was held fixed at $T_{P,burning} = 900$ K (Anthenien *et al.* 2006).

The evolution of the instantaneous mass of the particle (m_P) is calculated using an effective mass diameter (D_{eff}) and its rate of decrease with time as prescribed by the following equations (Tse and Fernandez-Pello 1998; Anthenien *et al.* 2006):

$$D_{eff} = [m_P/(\rho_{P,0}\pi/6)]^{1/3}; \quad \frac{d(D_{eff}^2)}{dt} = -\beta_0 (1 + 0.276\,\mathrm{Re}^{1/2}\,\mathrm{Pr}^{1/3}) \quad (16)$$

In this equation, $\rho_{P,0}$ is the initial density of the firebrand and β_0 is a quiescent atmosphere burning constant. $\mathrm{Pr} = (\mu_{film} c_{P,film} \div k_{film})$ is the Prandtl number of air. Re is a Reynolds number based on the diameter of a sphere with volume equal to the volume of the particle, $d_v = (3b\ D_P^2)^{1/3}$: $\mathrm{Re} = \rho_{air,film}\ d_v |\vec{V}_{rel}| \div \mu_{air,film}$. The values of $\beta_0 = 4.8 \times 10^{-7}$ m^2 s^{-1} and 1.8×10^{-7} m^2 s^{-1} have been proposed by Tse and Fernandez-Pello (1998) and Anthenien *et al.* (2006). In this work, based on a retuning of the model constants with reference to the experimental data of Tarifa *et al.* (1967) for stationary cylindrical particles of oak burned in a wind tunnel, the following value was found to provide the most satisfactory overall predictions: $\beta_0 = 3.42 \times 10^{-7}$ m^2 s^{-1}.

The evolution of the actual instantaneous diameter (D_P) of the burning cylindrical particles is assumed to be governed by the following equation, adapted from the work of Anthenien *et al.* (2006):

$$\frac{dD_P^4}{dt} = -\frac{C}{E} \left[\beta_0 (1 + 0.276\ \mathrm{Re}^{1/2}\,\mathrm{Pr}^{1/3}) \right]^2 t; \quad E = (L_P/D_P) \quad (17)$$

In the above equation, $L_P = 2b$ is the length of the cylindrical firebrand (which is assumed to remain essentially invariant), E is its instantaneous aspect ratio (length-to-diameter) and C is a model constant determined using experimental data. In the work of Anthenien *et al.* (2006), the initial aspect ratio, $E_0 = (L_P \div D_P)_o$, is used instead of E, and $C = 2\sqrt{3} = 3.464$ is recommended, in conjunction with $\beta_0 = 1.8 \times 10^{-7}$ m^2 s^{-1}. However, in this work, the aforementioned prescriptions of Anthenien *et al.* (2006) yielded relatively slow decay of ($m_P \div m_{P,0}$) and overly fast reduction of D_P to zero, vis-à-vis the corresponding experimental data of Tarifa *et al.* (1967). Thus, based on an extensive retuning exercise, the combination of $\beta_0 = 3.42 \times 10^{-7}$ m^2 s^{-1}, E (not E_0) and $C = 0.88\sqrt{3} = 1.5242$ was found to provide the most satisfactory overall predictions.

Burning cylindrical firebrands may extinguish with some mass remaining, as is the case when a residual char is formed as the wood smoulders. In such cases, the ratio of the residual to initial mass of the firebrand ($m_P \div m_{P,0}$) varies between 0 and 0.24 (Anthenien *et al.* 2006). A model for the cooling of

Fig. 3. Experimental setup at the Forest Fire Research Laboratory for Test Problem 1. Distance from the dropping point to the ground was 8.7 m.

extinguished firebrands was included in the present overall prediction procedure. However, in all cases considered in this work (test and demonstration problems), the firebrands did not attain values of $(m_P \div m_{P,0}) \leq 0.24$. Thus, it was not necessary to invoke the aforementioned cooling model in the final simulations.

Note on numerical solution of the proposed models

A fourth-order Runge–Kutta scheme was used for the numerical solution of Eqns 2–15 that govern the trajectory, orientation and angular velocity of the cylindrical particles in the prevailing wind, as well as Eqns 16 and 17 that represent their mass and size evolutions when they are burning. The time step, Δt, adopted in this Runge–Kutta numerical integration procedure was prescribed as a function of the particle local Stokes number (ratio of particle to fluid characteristic relaxation times). However, an upper limit (Δt_{max}) was also incorporated to ensure time-step independence of the results and numerical stability of the (explicit type) Runge–Kutta scheme.

Experiments with non-burning cylindrical particles falling in still air

Experiments with cylindrical particles falling in still air were undertaken inside the main hall of the Forest Fire Research Laboratory, which has a maximum height of 10 m, to obtain data that could be used in validation tests of the particle-tracking aspects of the proposed mathematical models (referred to as Test Problem 1 in the next section). In these experiments, 12 cylindrical particles of balsa wood (average value of mass density $\rho_P = 215.5\,\mathrm{kg\,m^{-3}}$) were dropped, with zero initial velocity, from a platform lift located 8.7 m above ground level (limiting value for which still air conditions could be imposed). The choice of balsa wood (instead of oak or some other wood that is more likely to be found in spot-fire conditions) was motivated by the aforementioned limitation in height: because particles of balsa are lighter than those of oak for the same dimensions, they take more time to travel through the air and reach the ground, thus decreasing the relative error made when measuring the total time of fall of the particles. The 12 cylindrical particles had identical radii ($a = 5$ mm) and three different half-lengths ($b = 30$, 40 and 50 mm; three groups of four cylindrical particles, each of same b). Using a particle-fixing device, the initial orientation of all particles was prescribed as follows: $\theta_0 = 60°$, $\varphi_0 = \psi_0 = 0$ (particles in the y–z plane, see Figs 2, 3). Each experiment was repeated, in a random order, at least three times. In each case, the trajectory of the cylinder was recorded using three video cameras aligned along the three axes of the inertial Cartesian coordinate system represented in Figs 2*a* and 3.

The experimental setup is displayed in Fig. 3. Video images for each test were captured using a digital camera (Sony DCR-SR87E HDD, MRA – instrumentations, Portugal) with 25 frames per second, and analysed using computer-aided-design (CAD) software, with frames separated in time by 0.2 s. Each video camera was operated manually to follow the movement of the particles using the highest possible image magnification. For certain conditions, the falling particle went out of the field of view of the camera, so the video recording could not follow the corresponding movement. For this reason, analyses of the video images were restricted to the first 5 m of particle fall, and used for determining the trajectories of the particle centre of mass and particle orientation. No discernible movement of the particle

Table 1. Experimental measurements and numerical predictions of the total time of fall (t_f) in still air for non-burning cylindrical balsa-wood particles of radius $a = 5$ mm and different values of half-length (b) released from a height of 8.7 m (results for Test Problem 1)

Particle half-length b (mm)	Aspect ratio $\beta = b \div a$	Total time of fall, t_f (s)	
		Experimental data	Numerical results
30	6	1.80	2.05
40	8	1.70	2.06
50	10	1.70	1.99

along the x-axis was observed (see Fig. 3). The value of t_f was also measured for each particle, with an uncertainty of less than ± 0.05 s.

Results and discussion

Two test problems and their results, which were used to validate the particle tracking and burning aspects of the proposed models for the cylindrical firebrands, are presented and discussed first in this section. After that, numerical predictions of simultaneous three-dimensional trajectories and mass and size evolutions of cylindrical wind-driven firebrands are presented and discussed for a demonstration problem.

Test problem 1: tracking of non-burning cylindrical particles falling in still air

In this test problem, the experimental measurements described in the last section were used to validate the particle-tracking aspects of the proposed models. A total of 12 non-burning cylindrical particles made of balsa wood were considered in the experiments and in the numerical simulations. Other details of this test problem are provided in the previous section, so they are not repeated here.

Experimental measurements and numerical predictions of the total time of fall, t_f, are presented in Table 1: the numerical predictions are a bit higher than the corresponding experimental measurements. Visual representations of the experimental recording and numerical prediction of the trajectory and angular orientation of one of the cylindrical particles ($a = 5$ mm and $b = 40$ mm) are presented in Fig. 4*a*,*b*. As was noted above, only the first 5 m of the particle trajectory could be recorded in the experiments. The experimental results presented in Fig. 4*a* show that the cylindrical particle initially oscillates about the horizontal orientation, the amplitude of these oscillations increases with time and the particle eventually starts rotating. The numerical predictions are able to capture the initial oscillations of the particle, but their amplitude is under-predicted and therefore the transition from particle oscillation to rotation is slightly delayed. The aforementioned differences between the experimental measurements and the corresponding numerical predictions were deemed as acceptable, in the context of the significant scatter in similar predictions yielded by various models for the drag and lift forces exerted on non-spherical particles moving in a fluid stream (Mandø and Rosendhal 2010). It should also be noted that a comparative evaluation of these models or their fine tuning to match the aforementioned experimental results were not within the scope of the work reported in this paper.

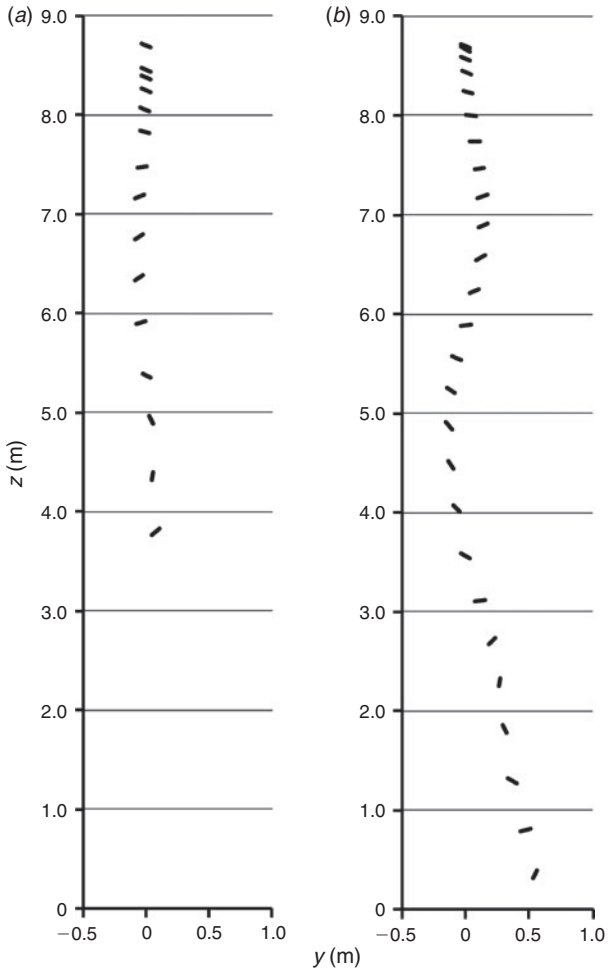

Fig. 4. Visual representations of the trajectory and angular orientation of one of the cylindrical particles ($a = 5$ mm and $b = 40$ mm) in Test Problem 1: (*a*) experimental measurements; and (*b*) numerical predictions.

Test problem 2: time evolution of the mass and size of stationary burning cylindrical particles inside a wind tunnel

In this test problem, time evolution of the mass and size of stationary cylindrical particles ($\vec{V}_P = 0$) of oak burning uniformly in flows of air inside a wind tunnel were considered. Comparisons of the experimental data of Tarifa *et al.* (1967) and the numerical predictions obtained with the proposed models are presented in Fig. 5*a*,*b*. In these figures, the experimental data for ($A_P \div A_{P,0}$) and ($m_P \div m_{P,0}$) are indicated as Series 1 and 2; and the corresponding (present) numerical predictions are indicated as Series 3 and 4. The experimental data of Tarifa *et al.* (1967) were taken from the work of Anthenien *et al.* (2006). The oak wood was assigned the following properties (Anthenien *et al.* 2006): mass density, $\rho_{oak} = 545\ \mathrm{kg\,m^{-3}}$; specific heat at constant pressure, $c_{p,oak} = 1466\ \mathrm{J\,kg^{-1}\,K^{-1}}$; and surface temperature of burning particle, $T_{P,burning} = 900$ K. The temperature of air far from the burning particle was set at $T_{air,\infty} = 300$ K and the air pressure was taken to be one standard atmosphere. The results presented in Fig. 5*a* are for initial particle diameter $D_{P,0} = 2a = 10$ mm, particle length $L_P = 2b = 30$ mm and wind

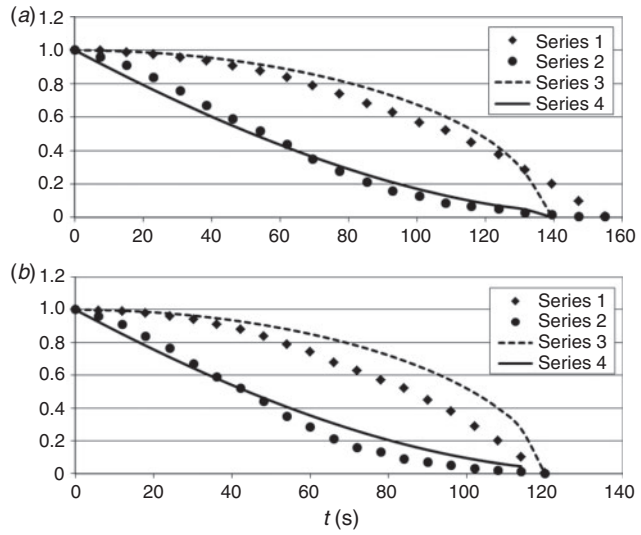

Fig. 5. Comparisons of the experimental data of Tarifa *et al.* (1967) for burning of stationary cylindrical particles ($\vec{V}_P = 0$) of oak in a wind tunnel, indicated as Series 1 for $A_P \div A_{P,0}$ and Series 2 for $m_P \div m_{P,0}$, with the corresponding (present) numerical predictions, indicated as Series 3 and Series 4 in Test Problem 2: (*a*) initial particle diameter $D_{P,0} = 2a = 10$ mm, particle length $L_P = 2b = 30$ mm and wind velocity $V_W = 2\ \mathrm{m\ s^{-1}}$; and (*b*) initial particle diameter $D_{P,0} = 2a = 15$ mm, particle length $L_P = 2b = 45$ mm, and wind velocity $V_W = 12\ \mathrm{m\ s^{-1}}$.

velocity $V_W = 2\ \mathrm{m\ s^{-1}}$; and the results presented in Fig. 5*b* are for initial particle diameter $D_{P,0} = 2a = 15$ mm, particle length $L_P = 2b = 45$ mm and wind velocity $V_W = 12\ \mathrm{m\ s^{-1}}$.

A uniform time step of 0.01 s was used in the final computations: the maximum values of the absolute differences in the corresponding results obtained with uniform time steps of 0.1 s were all less than 10^{-3}, relative to their initial values (unity). The results presented in Fig. 5*a*,*b* show that the present numerical predictions agree quite well with the corresponding experimental results of Tarifa *et al.* (1967).

Demonstration problem: trajectories and mass and size evolutions of cylindrical wind-driven firebrands

In this section, simultaneous predictions of three-dimensional trajectories and mass and size evolutions of firebrands transported in wind over a flat terrain, after they are effectively released from the fire plume, are presented and discussed. Four different cylindrical, uniformly burning, particles of oak, having the same initial volume $Vol_{P,0} = 8.0 \times 10^{-6}\ \mathrm{m^3}$ (and hence same initial mass) and surface temperature $T_{P,burning} = 900$ K, but different values of initial radius (a_0) and aspect ratio ($\beta_0 = b \div a_0$) were considered in this problem: Particle (i) with $a_0 = 7.97$ mm and $\beta_0 = 2.5$; Particle (ii) with $a_0 = 6.33$ mm and $\beta_0 = 5.0$; Particle (iii) with $a_0 = 5.02$ mm and $\beta_0 = 10.0$; and Particle (iv) with $a_0 = 3.99$ mm and $\beta_0 = 20.0$. The oak wood was assigned the following properties (Anthenien *et al.* 2006): mass density, $\rho_{oak} = 545\ \mathrm{kg\ m^{-3}}$; specific heat at constant pressure, $c_{p,oak} = 1466\ \mathrm{J\ kg^{-1}\ K^{-1}}$; and surface temperature of burning particle, $T_{P,burning} = 900$ K. The temperature of air far from the burning particle was set at $T_{air,\infty} = 300$ K and the air pressure was taken to be one standard atmosphere. The wind velocity profile was prescribed in accordance with Eqn 1, with $z_0 = 0.1$ m and $V_{ref} = 0.579\ \mathrm{m\ s^{-1}}$.

For each of the four firebrands, with reference to the notation in Fig. 2*a*, the centre of mass, *Cm*, was released from an initial location $\vec{x}_0 = [0.1\ \mathrm{m},\ 0.1\ \mathrm{m},\ 200\ \mathrm{m}]$, with zero initial velocity. However, to assess the influence of the initial orientation of the particle (with respect to the relative wind velocity vector) on its subsequent trajectory, the following three different release conditions were considered for each of the four particles, with respect to the notations in Fig. 2*a*,*b*: (1) in the vertical plane $x = 0.1$ m with ($\theta_0 = 60°$, $\varphi_0 = 0$, $\psi_0 = 0$); (2) in the vertical plane $y = 0.1$ m with ($\theta_0 = 60°$, $\varphi_0 = 90°$, $\psi_0 = 0$); and (3) in a vertical plane that is at an angle of 45° with the vertical planes $x = 0.1$ m and $y = 0.1$ m, with ($\theta_0 = 60°$, $\varphi_0 = 45°$, $\psi_0 = 0$). It should be noted that with the aforementioned prescription of the wind velocity profile, the wind speed at $z_{ini} = 200$ m is $11.0\ \mathrm{m\ s^{-1}}$.

At the relatively high initial release point ($z_{ini} = 200$ m; $t = 0$ s), each particle is supposed to have been previously lofted and ignited by the fire plume, so that it is considered to be fully burning. The aforementioned initial release height is consistent with the authors' observations in large fires in Portugal (Viegas *et al.* 2012), in which plume heights of the order of 600 m and spotting distances ranging from 200 to 1000 m were registered for firebrands produced by oak tree branches and twigs.

For the whole tracking and burning procedure, numerical stability was ensured and relative absolute differences (between corresponding results) of less than 10^{-3} were obtained with time steps of $\Delta t = 0.01$ s, 0.005 s and 0.001 s. All final computations were done with $\Delta t = 0.005$ s. The results are presented in the remainder of this section.

As a sample, with respect to the notation in Fig. 2*a*,*b*, the trajectories of the centroid of Particle (ii) in the z–x and z–y planes are shown in Fig. 6*a*,*b*, for the case in which this particle was initially located in the vertical plane $y = 0.1$ m with orientation ($\theta_0 = 60°$, $\varphi_0 = 90°$, $\psi_0 = 0$). The horizontal distance travelled between the release and landing locations was $d_h = 55.10$ m and the total time of fall was $t_f = 9.17$ s. The lateral drift along the y-axis was comparatively negligible. For the same case, the time-evolution of the particle angle of incidence (α_i) and the angle between its major axis (z' axis in Fig. 2*a*,*b*) and the horizontal plane ($\lambda = 90 - \theta$) are presented in Fig. 6*b*. A state of nearly time-periodic oscillation (but with amplitude increasing with time) of the angle (λ) is attained after approximately $t = 6$ s into the fall of the particle.

The time-evolution of the normalised particle mass ($m_P \div m_{P,0}$) for Particles (i) to (iv), all located initially in the vertical plane $y = 0.1$ m with orientation ($\theta_0 = 60°$, $\varphi_0 = 90°$, $\psi_0 = 0$), are presented in Fig. 7. For these initial conditions, the particles have the highest values of total time of fall (t_f) and horizontal distance travelled (d_h). It should also be recalled that the Particles (i) to (iv) have the same values of initial mass ($m_{P,0}$), but different values of initial radius and aspect ratio (a_0 and β_0). Particle (iv) has the highest value of initial aspect ratio ($\beta_0 = 20.0$) and it also has the highest total time of fall ($t_f = 10.52$ s) and the longest horizontal distance travelled ($d_h = 76.10$ m). As was mentioned earlier in this paper, in the present model, firebrand extinction is assumed to occur when its normalised mass reaches the threshold value of $m_P \div m_{P,0} = 0.24$. The results presented in Fig. 7 clearly show that such

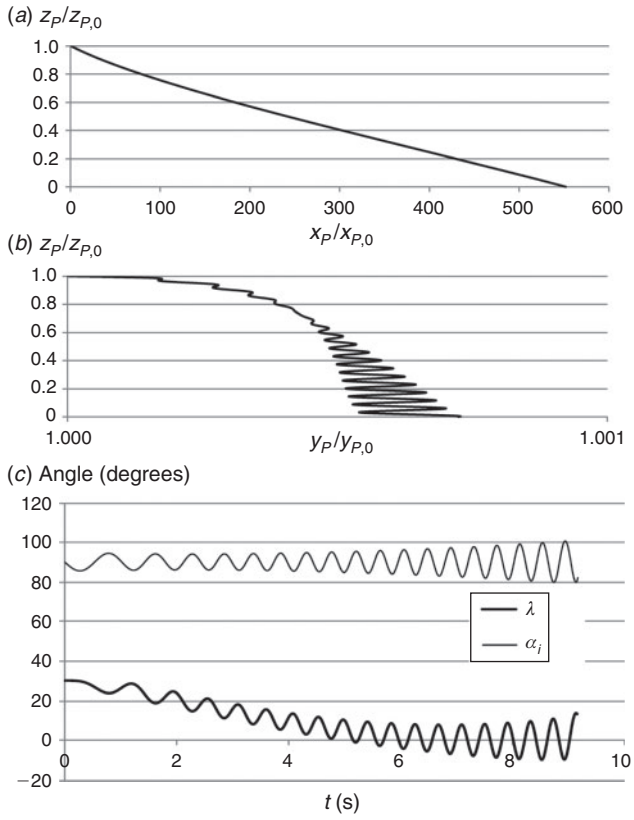

Fig. 6. Results for Particle (ii) in the demonstration problem ($z_{P,0} = 200$ m; $x_{P,0} = y_{P,0} = 0.1$ m; and particle located in the vertical plane $y = 0.1$ m with orientation ($\theta_0 = 60°$, $\varphi_0 = 90°$ and $\psi_0 = 0$): (*a*) trajectory of the particle centroid in the x–z plane; (*b*) trajectory of the particle centroid in the y–z plane; and (*c*) time-evolutions of the particle angle of incidence (α_i) and orientation with respect to the horizontal plane ($\lambda = 90 - \theta$). Schematic illustration of the notation is provided in Fig. 2.

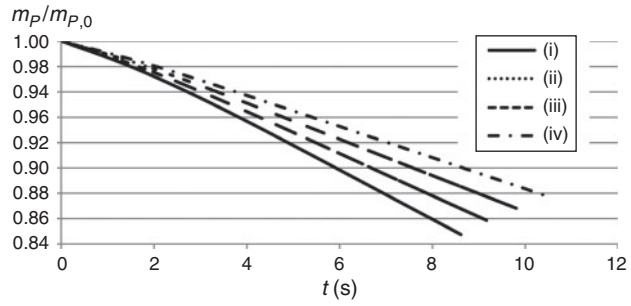

Fig. 7. Time evolution of the normalised particle mass ($m_P \div m_{P,0}$) for Particles (i) to (iv) in the demonstration problem, all particles located initially in the vertical plane $y = 0.1$ m with orientation ($\theta_0 = 60°$, $\varphi_0 = 90°$, $\psi_0 = 0$).

a threshold was not attained by any particle in the present simulations. Accordingly, it was not necessary to invoke a particle cooling procedure in the proposed overall model, and the firebrand temperature remained constant, namely, $T_{P,burning} = 900$ K.

The influences of the aforementioned three different initial orientations of the particles on their subsequent trajectories are illustrated by the values of t_f and d_h presented in Table 2. These results show that even though the values of initial volume (and hence mass) of Particles (i) to (iv) were the same, both the horizontal distance travelled and the total time of fall increase – although not linearly – with the initial aspect ratio ($\beta_0 = b \div a_0$) for all three initial orientations. This finding is in agreement with what is observed in actual forest fires: long firebrands, like pieces of eucalyptus bark, are known to achieve spotting distances up to 10 km from the main fire and in some instances even higher values (McArthur 1967; Cheney and Bary 1969). The results presented in Table 2 also show that the initial orientation of the particle (and hence its subsequent oscillations and possible rotation) play an important role in determining its trajectory (falling history). For example, for Particle (iv), which has $\beta_0 = 20$, changing its initial orientation from the vertical plane $x = 0.1$ m with ($\theta_0 = 60°$, $\varphi_0 = 0$, $\psi_0 = 0$) to the vertical plane $y = 0.1$ m with ($\theta_0 = 60°$, $\varphi_0 = 90°$, $\psi_0 = 0$) more than doubles the horizontal distance it travels, from $d_h = 36.2$ m to $d_h = 76.1$ m. The results for the other three particles are similar. These results show that accounting for initial orientation and the subsequent oscillations (and possible rotation) in the firebrand transport models is important when performing simulations for predictions of fire spread by spotting.

Table 2. Dependence of the total horizontal distance travelled (d_h) and time of fall (t_f) on initial orientation (notation is schematically illustrated in Fig. 2) for Particles (i) to (iv) in the demonstration problem

Initial orientation			Particle (i)		Particle (ii)		Particle (iii)		Particle (iv)	
θ_0	φ_0	ψ_0	d_h (m)	t_f (s)	d_h (m)	t_f (s)	d_h (m)	t_f (s)	d_h (m)	t_f (s)
60°	0°	0°	27.1	7.57	28.9	7.62	32.0	7.67	36.2	7.89
60°	45°	0°	37.1	8.07	42.7	8.32	48.0	8.52	53.2	8.73
60°	90°	0°	46.0	8.61	55.1	9.17	65.2	9.81	76.1	10.5

Concluding remarks

The main focus and the novel aspects of this work are related to (1) accounting for the oscillations (including possible rotation) of cylindrical wind-driven firebrands in relatively simple, but practical, mathematical models for predicting their trajectories and time-evolutions of mass and size; and (2) providing an assessment of the effects of these phenomena and the initial orientation of wind-driven firebrands on their total time of fall and horizontal distance travelled.

The proposed models were first validated by applying them to two test problems. In the first test problem, experimental measurements performed for non-burning cylindrical particles of balsa wood falling in still air were compared to the numerical predictions. The agreement between these results was found to be quite good, at least qualitatively. In the second test problem, numerical predictions of the time-evolution of mass and size of stationary burning cylindrical particles of oak in air flows inside a wind tunnel were compared with experimental results available in the literature. The agreement between these results was found to be good qualitatively and quantitatively.

The proposed models were then applied to a demonstration problem involving cylindrical wind-driven firebrands of oak

wood, with the same initial mass, volume and centre-of-mass position, but different values of the initial aspect ratio and initial orientation relative to the wind velocity. In this demonstration problem, the distance travelled by the firebrands from release to landing locations was found to be an increasing function of the initial aspect ratio. The initial orientation of the particles and their subsequent oscillations (and possible rotation) had significant influences on their trajectory. These results highlight the importance of accounting for particle oscillation and rotation in mathematical models that are employed for predicting fire spread by wind-borne firebrands. However, it should be noted that the present results were obtained for a rather limited range of parameters, for wind-driven cylindrical firebrands transported over flat terrains. Systematic investigations over a more complete range of parameters, in winds over uneven terrains (Lopes 2003), are necessary to provide further insights into this complex problem. The proposed models and procedures could be very useful in such investigations.

Acknowledgements

The support provided to the present research by the *Fundação para a Ciência e a Tecnologia* (FCT) through Projects SPOTFIRE (PTDC/EME-MFE/73765/2006), EXTREME (PTDC/EME-MFE/114343/2009) and PLURIANNUAL (PEst-OE/EME/LA0022/2013) is gratefully acknowledged. The authors also thank their colleagues J. P. Pinto and J. Raposo for their support in the implementation of the experimental setup for studying the fall of cylindrical particles in still air and also in other aspects of this work.

References

Ahrens CD (2009) 'Meteorology Today: an Introduction to Weather, Climate, and the Environment', 9th edn. (Brooks/Cole: Belmont, CA)

Albini FA, Alexander ME, Cruz MG (2012) A mathematical model for predicting the maximum potential spotting distance from a crown fire. *International Journal of Wildland Fire* **21**, 609–627. doi:10.1071/WF11020

Almeida M, Viegas DX, Miranda AI, Reva V (2009) Combustibility of potential embers. In 'Proceedings of the 18th World IMACS/MODSIM Congress', 13–17 July 2009, Cairns, Australia. (Eds RS Anderssen, RD Braddock, LTH Newham) pp. 1–7. (Modelling and Simulation Society of Australia and New Zealand: Canberra, ACT) Available at http://www.mssanz.org.au/modsim09/Z1/almeida_m.pdf [Verified 3 June 2014]

Anthenien RA, Tse SD, Fernandez-Pello AC (2006) On the trajectories of embers initially elevated or lofted by small scale ground fire plumes in high winds. *Fire Safety Journal* **41**, 349–363. doi:10.1016/J.FIRESAF.2006.01.005

Cheney NP, Bary GAV (1969) The propagation of mass conflagrations in a standing eucalypt forest by the spotting process. In 'Mass Fire Symposium: Collected Papers', 10–12 February 1969, Canberra, ACT. Vol. 1, Paper A6. (Commonwealth of Australia, Defence Standard Laboratories: Melbourne)

Ellis PF (2000) The aerodynamic and combustion characteristics of eucalypt bark – a firebrand study. PhD thesis, Australian National University, Canberra.

Ganser GH (1993) A rational approach to drag prediction of spherical and non-spherical particles. *Powder Technology* **77**, 143–152. doi:10.1016/0032-5910(93)80051-B

Goldstein H, Poole C, Safko J (2002) 'Classical Mechanics', 3rd edn. (Addison-Wesley: New York)

Himoto K, Tanaka T (2005) Transport of disk-shaped firebrands in a turbulent boundary layer. In 'Eighth International Symposium on Fire Safety Science', 18–23 September 2005, Beijing, China. (Eds DT Gottuk, BY Lattimer) pp. 433–444. (International Association for Fire Safety Science: Baltimore, MD)

Hoerner, SF (1965) 'Fluid-Dynamic Drag.' (S.F. Hoerner: Bakersfield, CA)

Hölzer A, Sommerfeld M (2008) New simple correlation formula for the drag coefficient of non-spherical particles. *Powder Technology* **184**, 361–365. doi:10.1016/J.POWTEC.2007.08.021

Incropera FP, DeWitt DP (1996) 'Fundamentals of Heat and Mass Transfer', 4th edn. (Wiley: New York)

Kelbaliyev GI (2011) Drag coefficients of variously shaped solid particles, drops, and bubbles. *Theoretical Foundations of Chemical Engineering* **45**, 248–266. doi:10.1134/S0040579511020084

Knight IK (2001) The design and construction of a vertical wind tunnel for the study of untethered firebrands in flight. *Fire Technology* **37**, 87–100. doi:10.1023/A:1011605719943

Koo E, Pagni PJ, Weise DR, Woycheese JP (2010) Firebrands and spotting ignition in large-scale fires. *International Journal of Wildland Fire* **19**, 818–843. doi:10.1071/WF07119

Koo E, Linn RR, Pagni PJ, Edminster CB (2012) Modelling firebrand transport in wildfires using HIGRAD/FIRETEC. *International Journal of Wildland Fire* **21**, 396–417. doi:10.1071/WF09146

Kortas S, Mindykowski P, Conslavi JL, Mhiri H, Porterie B (2009) Experimental validation of a numerical model for the transport of firebrands. *Fire Safety Journal* **44**, 1095–1102. doi:10.1016/J.FIRESAF.2009.08.001

Lopes AMG (2003) WindStation – a software for the simulation of atmospheric flows over complex topography. *Environmental Modelling & Software* **18**, 81–96. doi:10.1016/S1364-8152(02)00024-5

Lopes AMG, Sousa ACM, Viegas DX (1995) Numerical simulation of turbulent flow and fire propagation in complex topography. *Numerical Heat Transfer Part A* **27**, 229–253. doi:10.1080/10407789508913698

Mandø M, Rosendhal L (2010) On the motion of non-spherical particles at high Reynolds number. *Powder Technology* **202**, 1–13. doi:10.1016/J.POWTEC.2010.05.001

Manzello SL, Shields JR, Yang JC, Hayashi Y, Nii D (2007) On the use of a firebrand generator to investigate the ignition of structures in wildland-urban interface (WUI) fires. In 'Proceedings of 11th International Conference on Fire Science and Engineering (INTERLFAM)', 3–5 September 2007, London. pp. 862–872. (Interscience Communications: London)

Manzello SL, Shields JR, Cleary TG, Maranghides A, Mell WE, Yang JC, Hayashi Y, Nii D, Kurita T (2008) On the development and characterization of a firebrand generator. *Fire Safety Journal* **43**, 258–268. doi:10.1016/J.FIRESAF.2007.10.001

Manzello SL, Hayashi Y, Yoneki T, Yamamoto Y (2010) Quantifying the vulnerabilities of ceramic tile roofing assemblies to ignition during a firebrand attack. *Fire Safety Journal* **45**, 35–43. doi:10.1016/J.FIRESAF.2009.09.002

Manzello SL, Park S-H, Suzuki S, Shields JR, Hayashi Y (2011) Experimental investigation of structure vulnerabilities to firebrand showers. *Fire Safety Journal* **46**, 568–578. doi:10.1016/J.FIRESAF.2011.09.003

Manzello SL, Suzuki S, Hayashi Y (2012*a*) Exposing siding treatments, walls fitted with eaves, and glazing assemblies to firebrand showers. *Fire Safety Journal* **50**, 25–34. doi:10.1016/J.FIRESAF.2012.01.006

Manzello SL, Suzuki S, Hayashi Y (2012*b*) Enabling the study of structure vulnerabilities to ignition from wind driven firebrand showers: a summary of experimental results. *Fire Safety Journal* **54**, 181–196. doi:10.1016/J.FIRESAF.2012.06.012

Marchildon EK, Clamen A, Gauvin WH (1964) Drag and oscillatory motion of freely falling cylindrical particles. *Canadian Journal of Chemical Engineering* **42**, 178–182. doi:10.1002/CJCE.5450420410

McArthur AG (1967) Fire behaviour in eucalypt forests. Commonwealth of Australia, Forest and Timber Bureau, Leaflet number 107. (Canberra, ACT)

McRae GJ, Goodin WR, Seinfeld JH (1982) Development of a second-generation mathematical model for urban air pollution. I. Model formulation. *Atmospheric Environment* **16**, 679–696. doi:10.1016/0004-6981(82)90386-9

Mell W, Maranghides A, McDermott R, Manzello SL (2009) Numerical simulation and experiments of burning douglas fir trees. *Combustion and Flame* **156**, 2023–2041. doi:10.1016/J.COMBUSTFLAME.2009.06.015

Muraszew A, Fedele JB (1977) Trajectory of firebrands in and out of fire whirls. *Combustion and Flame* **30**, 321–324. doi:10.1016/0010-2180(77)90081-5

Ohmiya Y, Iwami T (2000) An investigation on the distribution of firebrands and spot fires due to a hotel fire. *Fire Science & Technology* **20**, 27–35. doi:10.3210/FST.20.27

Oliveira LA, Costa VAF, Baliga BR (2008) Numerical model for the prediction of dilute, three-dimensional, turbulent fluid-particle flows, using a Lagrangian approach for particle tracking and a CVFEM for the carrier phase. *International Journal for Numerical Methods in Fluids* **58**, 473–491. doi:10.1002/FLD.1729

Porteiro J, Míguez JL, Granada E, Moran JC (2006) Mathematical modelling of the combustion of a single wood particle. *Fuel Processing Technology* **87**, 169–175. doi:10.1016/J.FUPROC.2005.08.012

Porterie B, Consalvi JL, Kaiss A, Loraud JC (2005) Predicting wildland fire behavior and emissions using a fine-scale physical model. *Numerical Heat Transfer Part A* **47**, 571–591. doi:10.1080/10407780590891362

Ren B, Zhong W, Jin B, Lu Y, Chen X, Xiao R (2011) Study on the drag of a cylinder-shaped particle in steady upward gas flow. *Industrial & Engineering Chemistry Research* **50**, 7593–7600. doi:10.1021/IE102263U

Roberts AF (1970) A review of kinetics data for the pyrolysis of wood and related substances. *Combustion and Flame* **14**, 261–272. doi:10.1016/S0010-2180(70)80037-2

Sardoy N, Consalvi JL, Porterie B, Kaiss A (2006) Transport and combustion of ponderosa pine firebrands from isolated burning trees. In 'First International Symposium on Environment Identities and Mediterranean Area, 2006. ISEIMA '06', 9–12 July 2006, Corte-Ajaccio, France. pp. 6–11. (Institute of Electrical and Electronics Engineers: New York)

Sardoy N, Consalvi JL, Porterie B, Fernandez-Pello AC (2007) Modeling transport and combustion of firebrands from burning trees. *Combustion and Flame* **150**, 151–169. doi:10.1016/J.COMBUSTFLAME.2007.04.008

Sardoy N, Consalvi JL, Kaiss A, Fernandez-Pello AC, Porterie B (2008) Numerical study of ground-level distribution of firebrands generated by line fires. *Combustion and Flame* **154**, 478–488. doi:10.1016/J.COMBUSTFLAME.2008.05.006

Sullivan AL (2009*a*) Wildland surface fire spread modelling, 1990–2007. 1. Physical and quasi-physical models. *International Journal of Wildland Fire* **18**, 349–368. doi:10.1071/WF06143

Sullivan AL (2009*b*) Wildland surface fire spread modelling, 1990–2007. 2. Empirical and quasi-empirical models. *International Journal of Wildland Fire* **18**, 369–386. doi:10.1071/WF06142

Sullivan AL (2009*c*) Wildland surface fire spread modelling, 1990–2007. 3. Simulation and mathematical analogue models. *International Journal of Wildland Fire* **18**, 387–403. doi:10.1071/WF06144

Sullivan AL, Knight IK, Hurley RJ, Webber C (2013) A contractionless, low-turbulence wind tunnel for the study of free-burning fires. *Experimental Thermal and Fluid Science* **44**, 264–274. doi:10.1016/J.EXPTHERMFLUSCI.2012.06.018

Suzuki S, Manzello SL, Matthew Lage M, Laing G (2012) Firebrand generation data obtained from a full-scale structure burn. *International Journal of Wildland Fire* **21**, 961–968. doi:10.1071/WF11133

Tachikawa M, Fukuyama M (1981) Trajectories and velocities of typhoon-generated missiles. *Transactions of Architectural Institute of Japan* **302**, 1–11[In Japanese]

Tarifa CS, Del Notario PP, Moreno FG (1965) On the flight paths and lifetimes of burning particles of wood. *Proceedings of the Combustion Institute* **10**, 1021–1037. doi:10.1016/S0082-0784(65)80244-2

Tarifa CS, Del Notario PP, Moreno FG, Villa AR (1967) Transport and combustion of firebrands. USDA Forest Service, Final Report of Grant FG-SP-114 and FG-SP-146. (Madrid)

Tse SD, Fernandez-Pello AC (1998) On the flight paths of metal particles and embers generated by power lines in high winds – a potential source of wildland fires. *Fire Safety Journal* **30**, 333–356. doi:10.1016/S0379-7112(97)00050-7

Viegas DX (2002) Fire behaviour models: an overview. In 'Forest Fires: Ecology and Control, Atti del XXXIX Corso di Cultura in Ecologia', 2–6 September 2002, San Vito di Cadore, Italy. (Eds T Anfodillo, V Carraro) pp. 37–47. (Università Degli Studi di Padova) Available at http://www.incendiboschivi.org/docum/prevenz/fuocoinforest.pdf [Verified 3 June 2014]

Viegas DX (2004) A mathematical model for forest fires blowup. *Combustion Science and Technology* **177**, 27–51. doi:10.1080/00102200590883624

Viegas DX (2006) Parametric study of an eruptive fire behaviour model. *International Journal of Wildland Fire* **15**, 169–177. doi:10.1071/WF05050

Viegas DX, Gabbert W, Figueiredo AR, Almeida MA, Reva V, Ribeiro LM, Viegas MT, Oliveira R, Raposo JR (2012) Report on the Forest Fire of Tavira/São Brás de Alportel, 18–22 July 2012. Centro de Estudos sobre Incêndios Florestais, ADAI/LAETA, University of Coimbra. (Coimbra, Portugal) [In Portuguese]

Woycheese JP, Pagni PJ (1999) Combustion models for wooden brands. In 'Proceedings of 3rd International Conference on Fire Research and Engineering (ICFRE3)', 4–8 October 1999, Chicago, IL. pp. 53–71. (Society of Fire Protection Engineers, Boston, MA)

Yin C, Rosendahl L, Kær SK, Sorensen H (2003) Modelling the motion of cylindrical particles in a nonuniform flow. *Chemical Engineering Science* **58**, 3489–3498. doi:10.1016/S0009-2509(03)00214-8

Yin C, Rosendahl L, Kær SK, Condra TJ (2004) Use of numerical modeling in design for co-firing biomass in wall-fired burners. *Chemical Engineering Science* **59**, 3281–3292. doi:10.1016/J.CES.2004.04.036

Zastawny M, Mallouppas G, Zhao F, van Wachem B (2012) Derivation of drag and lift force and torque coefficients for non-spherical particles in flows. *International Journal of Multiphase Flow* **39**, 227–239. doi:10.1016/J.IJMULTIPHASEFLOW.2011.09.004

Zhou X, Mahalingam S, Weise D (2007) Experimental study and large eddy simulation of effect of terrain slope on marginal burning in shrub fuel beds. *Proceedings of the Combustion Institute* **31**, 2547–2555. doi:10.1016/J.PROCI.2006.07.222